Applied Surface Science 642 (2024) 158654

Contents lists available at ScienceDirect

Applied Surface Science

journal homepage: www.elsevier.com/locate/apsusc

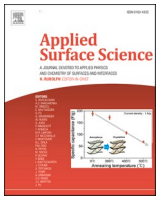

Full Length Article

A 2D-to-3D morphology transitions of gold in organic acid electrolytes: Characterization and application in bioanode design

Rokas Žalnėravičius [a,b,*], Arnas Naujokaitis [b], Vitalija Jasulaitienė [b], Rasa Rutkienė [a], Rolandas Meškys [a], Marius Dagys [a]

[a] Institute of Biochemistry, Life Sciences Center, Vilnius University, Saulėtekio av. 7, LT-10257 Vilnius, Lithuania
[b] Centre for Physical Sciences and Technology (FTMC), Sauletekio av. 3, LT-10257 Vilnius, Lithuania

ARTICLE INFO

Keywords:
Nanoporous gold
Gold anodization
Nanostructurisation
Direct electron transfer
Bioanode
Glucose dehydrogenase

ABSTRACT

The inexpensive, relatively fast and scalable production of nanostructured electrodes may benefit future disposable biosensor technology. In this research, nanoporous gold (NPG) surfaces were successfully fabricated by anodizing the gold in different organic acid, and further used for glucose dehydrogenase (GDH)-based bioanode design. The porosity of NPG layers was manipulated by changing the anodization time, and the dependency of relative electrochemical surface area (rESA) on the bioanode performances was systematically examined. The X-ray photoelectron spectroscopy (XPS) studies of NPG formed in oxalic acid (NPG_{ox}) and their depth profiles of Au 4f and O 1s evidenced the chemical state of pure metallic gold (Au^0), whereas NPG formed in glycolic acid (NPG_{gly}) has appreciable content of gold oxide and hydroxides. The NPG_{gly}/4-ATP/GDH bioanodes exhibited direct electron transfer (DET-type) bioelectrocatalytic activity, while the highest current densities of 0.35 mA cm^{-2} and low onset potential of −0.189 V (vs. Ag/AgCl) were observed. The electrodes showed long-term stability and, up to three weeks, retained 76 % of their initial value. Furthermore, the biofuel cell possessed the maximum power densities of 31.8 μW cm^{-2} and open-circuit potential (OCP) differences of 0.441 V, thus evidencing that NPG_{gly} layers could be encouraging for developing biosensors and biofuel cells.

1. Introduction

In enzymatic fuel cells (EFC), the purified enzymes isolated from various microorganisms were used as a biocatalyst at either or both electrodes [1]. The bioelectrode that oxidizes a fuel (i.e., glucose) is called a bioanode, which generates electrons and transfers them to the solid electrode (transducer layer). The released electrons then flow through the electric circuit to the (bio)cathode and are further consumed to drive the reduction reaction, i.e., O_2 reduction to H_2O [2]. In both compartments, the redox communication between enzyme co-factor and solid electrodes plays a major role in efficient EFC design and is identified as direct and mediated electron transfer (DET and MET). Regardless of the extensive research of more than half a century, there is still a dispute on whether DET or MET surpass each other in performance [3]. Theoretical insights support that in MET-type bioelectrocatalysis, bioelectrodes provide higher current or power densities because most of the immobilized enzymes can participate in the redox reaction [4]. However, for practical use in flow systems, i.e., to maintain the implantable low-energy biosensor device, the DET-type EFC enables the enzymes to operate at a potential closer to their standard redox potential, thus resulting in a higher open-circuit potential and offers higher stability and simpler design [5].

Despite the hundreds of papers dealing with DET, it was reported that in the class of oxidoreductases, only 100 of 1654 known enzymes could facilitate DET [6]. The main factors that limit the enzyme's DET-capability are their cofactor location, which is usually deeply buried within the enzyme's matrix and the short electron tunnelling distance (~10 Å) [7]. To enhance the DET-type reactions, a lot of efforts have been addressed, including enzyme engineering [8], its optimal orientation on electrode [9], immobilization technique [10] and nanostructurization of plain electrodes to ensure maximal enzyme loadings. Among the different approaches, the utilization of various nanomaterials, including metal-based nanoparticles [11], carbon nanostructures [12], conducting polymers [13] or porous materials [14], suggest a very prospective alternative to improve the DET rate.

Nanoporous gold (NPG) has attracted considerable attention due to

* Corresponding author at: Institute of Biochemistry, Life Sciences Center, Vilnius University, Saulėtekio av. 7, LT-10257 Vilnius, Lithuania.
E-mail address: rokas.zalneravicius@gmc.vu.lt (R. Žalnėravičius).

https://doi.org/10.1016/j.apsusc.2023.158654
Received 15 June 2023; Received in revised form 29 September 2023; Accepted 9 October 2023
Available online 11 October 2023

its remarkable features, such as high surface-to-volume ratio, 3D-conductive networks and biocompatibility [15]. These features make the NPG surfaces suitable for non-enzymatic glucose sensors [16], as well as a promising catalyst for hydrogen evolution reaction [17], CO_2 [18] and H_2O_2 reduction [19]. Recently, Takahashi et al. have shown that the immobilized bilirubin oxidase on NPG surfaces promotes bioelectrocatalytic activity, possibly by ensuring its more favourable orientation for efficient DET [20]. More recently, Bollella et al. have fabricated the highly porous gold (hPG) structures and further functionalized them with different thiols to form self-assembly monolayers (SAMs). They found that –OH groups on hPG structures help to stabilize and orientate the fructose dehydrogenase (FDH) enzyme layer on the surface of the electrode. The FDH/4-MPH/h-PG bioanode exhibited a current density of almost 1 mA cm^{-2} in the presence of 10 mM of fructose and maintained incredible stability over 90 days (retained activity of 90 %) [21]. Adachi et al. have reported the superior DET-type bioelectrocatalytic activity of FAD-dependant glucose dehydrogenase from A. terreus immobilized on NPG electrode and enzymatically implanted platinum nanoclusters. The constructed bioanode possesses approximately 1 mA cm^{-2} current densities at the potential of 0 V (vs Ag/AgCl) in the presence of 0.1 M glucose [22].

Generally, the NPG structures are formed by chemical and electrochemical dealloying/etching methods, whereas the sponge-like architectures are organized by dissolving less noble metals in gold alloys [21]. In some research, the NPG was fabricated by a simple anodization technique in Cl^- containing electrolytes [23,24]; however, the dimensions of gold nanostructures are higher than those observed by the pioneered research reported by Nisho et al., whereas the black nanoporous gold surfaces were produced by the gold anodization in oxalic acid [25]. This method is attractive due to its simplicity and its ability to create NPG thin films on the various forms of planar gold electrodes. Besides, this technique avoids some contaminations in NPG layers that usually arise from the alloying metals. This nanostructurization does not require extremely aggressive solutions that can completely damage some parts of the electrode, e.g., Ag-pseudo-reference electrode on gold-based screen-printed electrodes. Furthermore, it may help to pass a painful step that usually arises during the nanostructurization of bare gold by using gold nanoparticles, specifically when it has to be accurately drop-casted on bare gold electrode surfaces. Skip this step would positively impact the nanostructured electrode production, especially in scaling up. However, to date, there is a lack of knowledge about the formation of NPG by anodization in other organic acids. It was hypothesized that the anodization of bare gold in different organic acid solutions would possibly influence the surface morphology of NPG layers. Luckily, it could be more suitable for applications in biosensors and biofuel cells and thus deserves further investigation.

In this research, the gold anodization in four different organic electrolytes, in particular: oxalic, glycolic, citric and tartaric acids and their impact on the performance of bioanode based on glucose dehydrogenase immobilised on 4-aminothiophenol modified NPG electrodes have been extensively studied. Unexpectedly, it was revealed that the morphology of NPG surfaces highly depends on the applied organic acid during the anodization. The formed black, grey and orange porous thin films on the gold surfaces resulted in an enhanced relative electrochemical surface area (rESA) compared to planar gold. Furthermore, it was shown that NPG formed by anodizing the gold in glycolic acid (NPG_{gly}) reduced the round-shaped nanoparticles diameter by almost 20 nm compared to NPG produced in oxalic acid (NPG_{ox}). This decrease possibly leads to the higher immobilized enzyme coverage on NPG_{gly}; consequently, the approximately ~ 35 % higher bioelectrocatalytic current and almost two-fold higher power densities related to the bioelectrooxidation of glucose were obtained. These features indicate that NPG_{ox} and NPG_{gly} formation by one-step anodization makes it a promising approach for porous thin film formation on gold suitable for any biorecognition element immobilization.

2. Experimental section

2.1. Materials and chemical reagents

All chemical reagents used in this research were used as received without additional purification unless otherwise stated. Oxalic (99 %), glycolic (99 %), tartaric (99.5 %), citric (99 %), sulphuric (95–97 %) acids, potassium sulphate (99 %), potassium chloride (99 %), 4-aminothiophenol (4-ATP, 97 %), potassium hydroxide (85 %), multi-walled carbon nanotubes (CNT, diameter ranges from 6 to 13 nm, 98 %) and proton exchange membrane (PEM) Nafion 115 (125 μm thick) were provided by Sigma-Aldrich Chemical Co (USA). All salts, including sodium chloride (99 %), disodium hydrogen phosphate (99 %) and potassium dihydrogen phosphate (99 %) used for buffer preparation were obtained from Reachem Slovakia S.r.o (Slovakia). D, L-glucose (99 %), methanol (99 %), potassium hexacyanoferrate (II) (98 %) and potassium ferricyanide (III) (99 %) were purchased from Alfa Aesar (USA). The heme-containing membrane-bound glucose dehydrogenase (GDH) was excluded from Gram-negative bacteria of *Ewingella americana* and further characterized as described previously [26]. The stock solution of GDH (4 mg mL^{-1}) was diluted four-fold with 0.1 M PBS and further used for enzyme immobilization.

To achieve the equilibrium between α- and β- forms, the 1 M of glucose stock solution was prepared at least 24 h before usage and stored at 4 °C if not in use.

2.2. Cleaning of electrodes

Gold (GE) and glassy carbon (GC) electrodes with a geometric surface area of 0.0314 and 0.07065 cm^2 were used for NPG layer formation as well as to construct GDH-based bioelectrodes. Before the usage, both electrodes were mechanically and electrochemically cleaned. The bare GE surface was firstly polished by turs with 1.0 μm and 0.3 μm Al_2O_3 powder. The mirror-like electrodes were further ultrasonically cleaned in water for 6 min to remove the possible abrasives from the surface. Then, the GE electrodes were electrochemically cleaned by continuous cycling in the 0.05 M KOH and 0.5 M H_2SO_4 solutions at the potential ranges of 50 to 2650 mV and −400 to 1500 mV and a scan rate of 100 mV s^{-1}, respectively, until reproducible scans were obtained. It should be noted that after each preparation step, the electrodes were thoroughly rinsed with distilled water (DI) and dried under nitrogen flow. The GC electrode was cleaned by following a similar path except for the parts of potential cycling in alkaline solutions and sonication, which can be destructive for the electrode [27,28].

2.3. Fabrication of NPG electrodes and its electrochemical characterization

A one-pot anodization approach produced the NPG layer on the bare gold electrodes in four aqueous electrolytes containing organic acids: oxalic, glycolic, tartaric and citric. The reaction was performed in three and two-electrode configuration setups, whereas the bare gold acted as a working (anode) and Pt sheet (40 × 70 mm) as a counter (cathode). The Hg/Hg_2SO_4 (+651 mV vs SHE) reference electrode was used to avoid the Cl^- interference. The anodization was carried out in a thermostat-controlled bath filled with a particular, freshly prepared organic acid cooled down to 4 ± 1 °C under magnetic stirring at 150 rpm. The galvanostatic regime was maintained using power supply PeakTech 6227 (Germany). After the anodization, the NPG electrodes were carefully rinsed with DI water by immersing them for at least 30 min to remove excess organic acid from the porous structure.

2.4. GDH-based bioanode design

The main GDH-based bioanode formation steps are summarized in the schematic illustration (Fig. 1). The NPG electrodes were modified

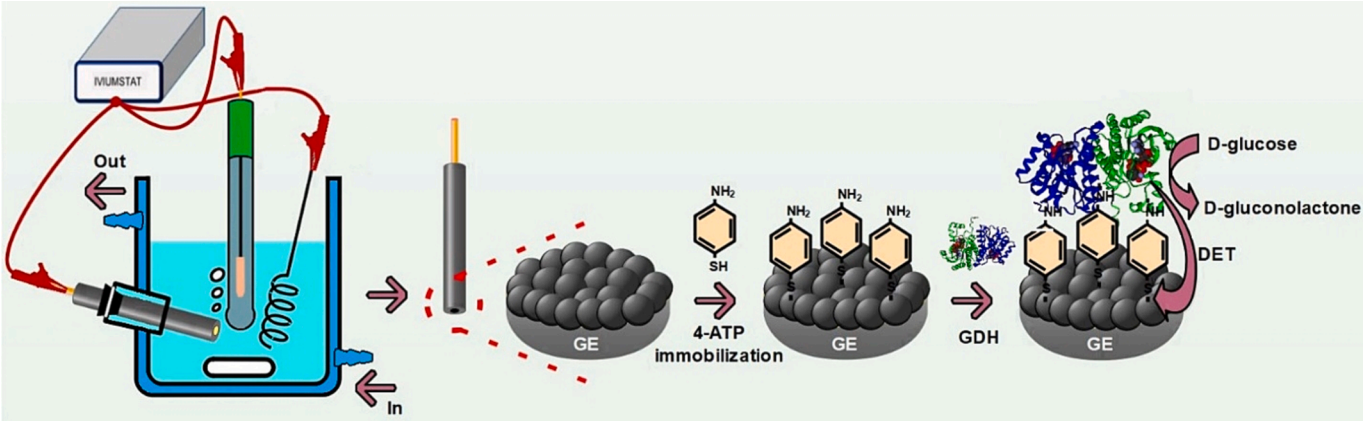

Fig. 1. Schematic representation of NPG/4-ATP/GDH bioanode preparation: electrochemical NPG formation and GDH immobilization on 4-ATP modified electrodes.

with 4-ATP molecules that form a self-assembly monolayer (SAM) on the surface and help to orientate the GDH enzyme, thus facilitating DET-type bioelectrocatalytic activity, as reported in our recent research [26]. To realize this, the NPG electrode was incubated in an N_2-saturated methanol solution containing 2 mM of 4-ATP and left for immobilization overnight. Finally, the NPG/4-ATP electrodes were enriched with biological catalyst by dropping 2.5 μL of 1 mg mL^{-1} GDH and kept for at least 2 h under humid conditions at 4 °C to avoid evaporation. After each preparation stage, the bioanode was carefully rinsed with 0.1 M PBS to eliminate non-adsorbed components. The designed bioanode was labelled NPG/4-ATP/GDH.

To prove the DET capability of the GDH enzyme, the GC electrode was modified with oxygen-containing groups enriched CNT. A detailed description of CNT functionalization can be found in our previous research [29]. The 5 μL of the dispersion of functionalized CNT (5 mg mL) was drop-casted on the electrode and left to dry at ambient conditions. Finally, 3 μL of GDH enzyme solution were dispersed on the surface of the GC/CNT electrode and left for immobilization under humid conditions at 4 °C for at least 2 h. The prepared electrodes were labelled as GC/CNT/GDH. All designed bioelectrodes were soaked into 0.1 M PBS buffer and stored at 4 °C if not used.

2.5. Electrochemical measurements

Notably, the electrode potentials in this study are referred to $Ag/AgCl_{3M\ KCl}$ electrode potential (+209 mV vs. SHE), including the cases when the Hg/Hg_2SO_4 electrode was used. A three-electrode configuration cell was used for most electrochemical measurements. The NPG electrode acted as a working, Ag/AgCl and Pt foil (12 × 35 mm) as a reference and counter electrode, respectively. The main electrochemical operations were carried out with a Zennium electrochemical workstation equipped with CVB 120 probe Zahner-Elektrik (Germany). All electrochemical investigations are described in SI.

2.6. Phase and morphology analysis of NPG surfaces

X-ray photoelectron spectroscopy (XPS) characterization of NPG surface electrochemically formed in 0.3 M oxalic and 1.8 M glycolic acids was carried out using Kratos AXIS Supra+ (UK) spectrometer with monochromatic Al K_α (1486.6 eV) X-ray radiation powered at 225 W. The base pressure in the analysis chamber was less than 1×10^{-9} mbar, and a low electron flood gun was used as a charge neutralizer. The survey spectra for each sample were recorded at a pass energy of −160 eV using a step size of 1 eV. High-resolution spectra were recorded using a pass energy of −10 eV and a step size of 0.1 eV overall individual element peaks. The binding energy scale was calibrated by setting the C1s hydrocarbon peak at 284.8 eV.

The monoatomic Ar^+ ions gun Minibeam 6 (UK) with an energy of 5 keV were used for continuous sputtering of NPG surfaces (scanned area of 2 × 2 mm) with intervals of 30 s. The effective sputtering rate was 3.2 nm/min measured at a SiO_2 reference sample.

The depth profile analysis consists of the 7 sputtering steps (30 s per one circle) until the content of carbon and oxygen are completely removed from the NPG surfaces. After each sputtering step, the high-resolution (HR) spectra were collected for Au, C and O, and the chemical composition was determined from corresponding XPS peak areas after inelastic background subtraction. All data were processed using the Avantage processing software ThermoScientific (UK). The area of the XPS analysis was 700 × 300 μm. Notably, for the XPS analysis, the GE specimens with a geometric surface area of ~1 cm^2 (~250 nm) were formed on mica pads coated by pure gold using the PVD 75 Kurt J. Lesker Company (USA) magnetron sputtering system. After anodization, electrodes were extensively washed with DI water, dried in N_2 flow and immediately subjected to XPS studies without additional purification.

The surface morphology and cross-section analysis of NPG electrodes were carried out by scanning electron microscope (SEM) Helios NanoLab 650 (Netherlands) supplied with a focused ion beam (FIB). The cross-section of NPG surfaces was made with a 30 keV Ga^+ ions beam.

3. Results and discussion

3.1. Morphology of NPG electrodes formed in oxalic, glycolic, tartaric and citric acids

In enzyme-based biosensors, biofuel cells and immunosensors, the nature of the underlying electrode can significantly influence the constructed device's performance and long-life stability properties. In this research, nanoporous gold (NPG) surfaces synthesized by one-pot gold anodization in oxalic acid are already known thanks to the pioneered work of Nishio et al. [25] and seem to be a promising technology for accurate bare gold nanostructurization. The overall morphology of NPG layers electrochemically formed in oxalic acid (NPG_{ox}) differs from those fabricated *via* the dealloying of Ag-Au alloys or other electrochemical pathways in Cl^- ion-containing electrolytes, whereas the size of the so-called ligament and crack usually are in the ranges of 40–50 nm [30]. The size of the oval-shaped nanoparticles on the NPG_{ox} structures exhibited an averaged diameter of 38 ± 1 nm and possessed overlapped and non-overlapped (as created by separated nanoparticles) morphology (Fig. 2 a). SEM analysis illustrates the 3D nanoporous structure of the randomly located porous with the averaged porous width of 56 nm. The NPG layers consist of interconnected gold nanoparticles with a size ranging from 27.5 to 47.5 nm (Fig. 2 a and S1 a). The thickness of black layered NPG mostly depends on the anodization time and applied regime: constant potential or current values. The 30

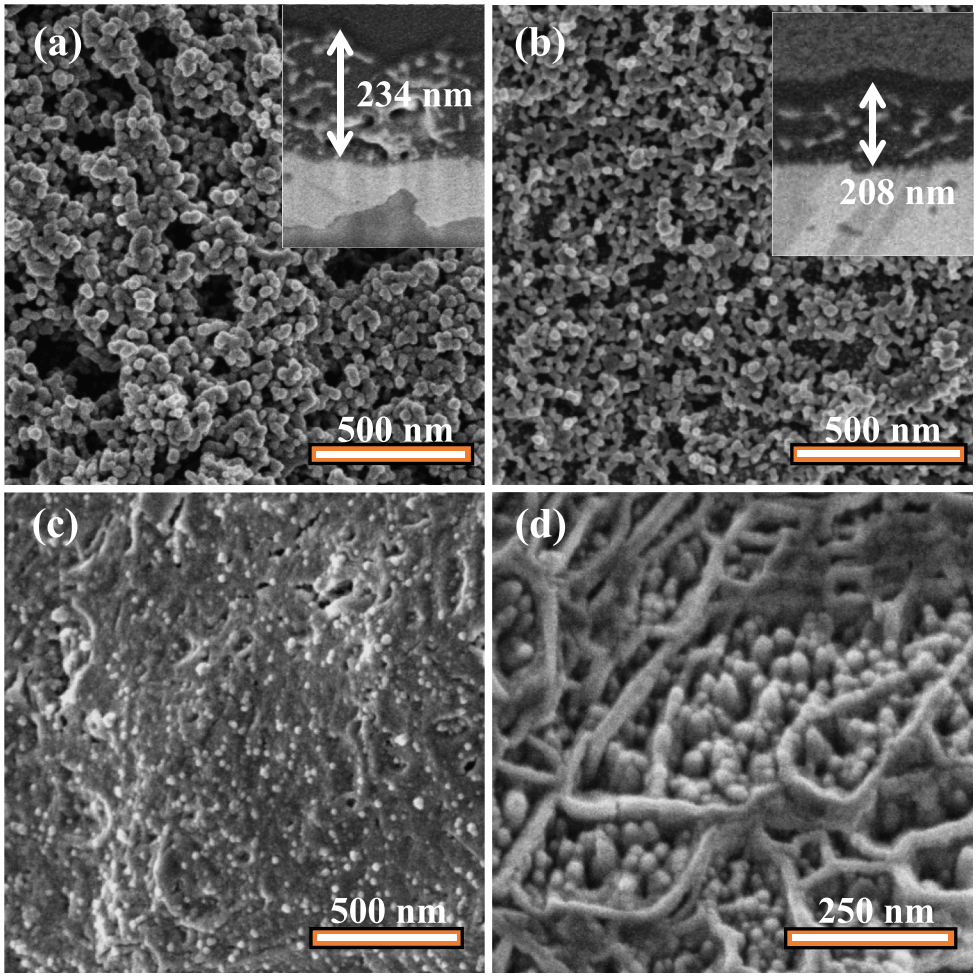

Fig. 2. Top-side SEM images of the nanostructured gold electrode after anodization in four different organic acid electrolytes for 30 min: (a) 0.3 M oxalic acid at 2.8 V, (b) 0.6 M glycolic acid, (c) 0.6 M tartaric acid and (d) 0.6 M citric acid at 3.8 V, respectively. *Insets*: cross-section SEM images of porous gold structures formed in oxalic (a) and glycolic (b) acids.

min of gold anodization in 0.3 M oxalic acid results in the black-coloured nanoporous layer formation with a thickness of ~ 230 nm (Fig. 2 a insets). However, it was observed that the mechanical strength of the NPG structures decreased by increasing the thickness of coatings and the anodizing of gold at the environmental temperature (20 °C). Since the mechanism of NPG_{ox} formation is not well understood, further developments in this field would be of great interest.

It was hypothesized that the chemical structure of organic acid could influence the NPG layer growth and probably its morphology. To verify this assumption, the organic acids containing 1 (glycolic), 2 (tartaric) and 3 (citric) carbonyl groups have been chosen herein. The grey and orange-coloured surfaces were obtained after the anodization of bare gold in a specified organic acid at 3.4 V for 30 min. The SEM images of NPG layers formed in glycolic, tartaric and citric acids revealed that NPG surface morphology highly depends on the applied organic acid, as illustrated in Fig. 2 b, c and d, respectively. The top-side SEM views of the layer formed in glycolic acid (Fig. 2 b) display that the grey film contains porous structures with an averaged pore diameter of 40 nm and the numerous round-shaped 20.1 nm sized nanoparticles which form a main NPG layer (Fig. S1 b).

To provide almost 20 nm smaller nanoparticles on bare gold surfaces by one-pot anodization of gold in glycolic acid solutions compared to traditional anodization in oxalic acid, to the best of our knowledge, has never been reported in scientific literature. The particle size of the NPG layer plays an essential role in developing DET-capable biosensors, biofuel cells or non-enzymatic glucose sensors [21,31]. Smaller nanoparticles could enhance the enzyme coverage, thus probably resulting in higher bioelectrode current and power densities.

Gold anodization in tartaric acid leads to the formation of orange films with randomly seeded nanoparticles with an averaged diameter of ~ 23 nm (Fig. 2 c). In contrast, the anodization of gold in citric acid forms orange films with irregularly shaped islands containing mountain-like structures with an average size of ~ 29 nm (Fig. 2 d). The differently nanostructured surfaces (four types) were further utilized as a transducer layer for bioanode construction to investigate the impact of surface morphology on the performance of DET-capable GDH.

3.2. Effect of applied organic acid and their impact on the DET performance of bioanodes

Since the nanostructurization of gold was accomplished by anodizing gold electrodes in four different organic acids, resulting in entirely various morphology of the NPG surfaces, the impact of applied organic acid on the DET performance of bioanode needs to be investigated. To realize this goal, four bare gold electrodes were anodized in freshly-prepared 0.3 M oxalic acid at 2.8 V for 30 min and in 0.6 M glycolic, tartaric and citric acids at 3.8 V for 1 h, respectively. The prolonged time (1 h) was chosen due to the much slower NPG growth on bare gold, as evidenced by rESA inspection (data not shown). Before the bioanode was constructed, the electrochemical characterization of bare and NPG electrodes was carried out. To determine the electrochemical surface area (ESA), the reduction current peak observed at 0.85–0.90 V (Fig. 3 a)

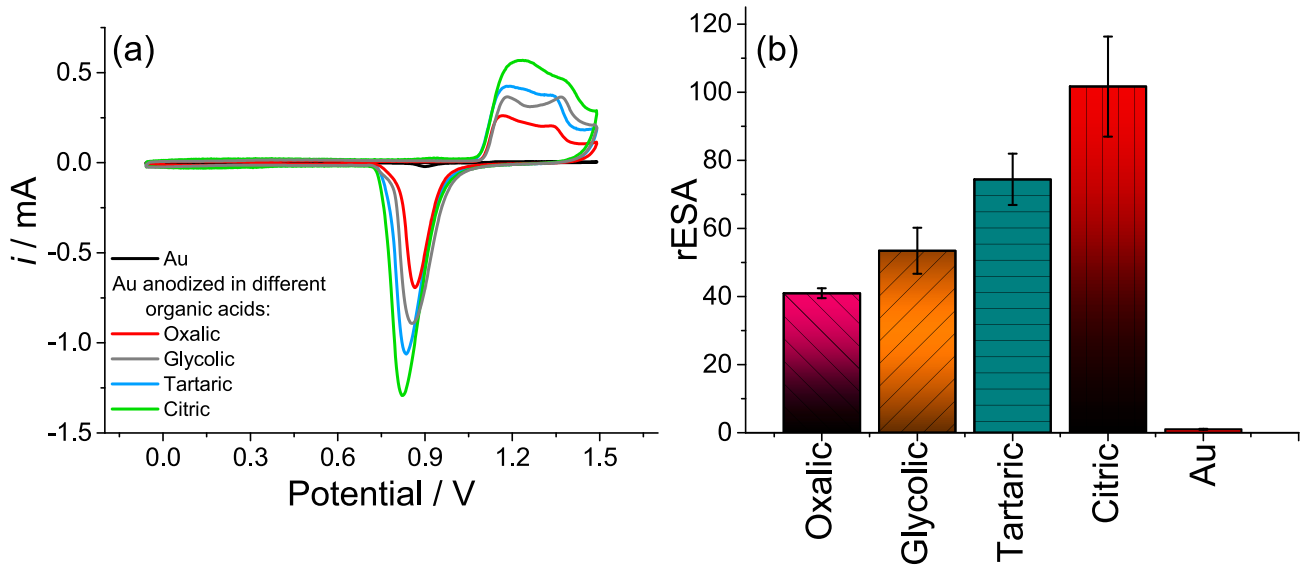

Fig. 3. Cyclic voltammograms of NPG electrodes (a) formed in different organic acid electrolytes: in 0.3 M oxalic at 2.8 V for 0.5 h; in 0.6 M glycolic, tartaric and citric acids at 3.8 V for 1.0 h, respectively. All CV curves were registered in 0.1 M H_2SO_4 at 50 mV s^{-1}. Histograms (b) show the relative (normalized with respect to bare gold) electrochemical surface area (rESA) of NPG electrodes synthesized in a specified electrolyte.

was integrated using OriginPro software, and the quantity of charge consumed to reduce gold oxides was calculated by applying the conversion factor of 390 μC cm^{-2} [32]. It was observed that nanostructurization of gold electrodes in oxalic acid occurred at higher rates compared to glycolic and tartaric acids, whereas the magnitude of relative ESA (rESA, normalized with respect to the ESA of bare gold) was higher only 1.3 and 1.8 fold even after two-fold extended anodization regime and higher applied potential (Fig. 3 b). In contrast, the highest rESA value of 101.65 was obtained after the anodizing of the gold electrode in citric acid, which provides almost 2.5 fold higher rESA

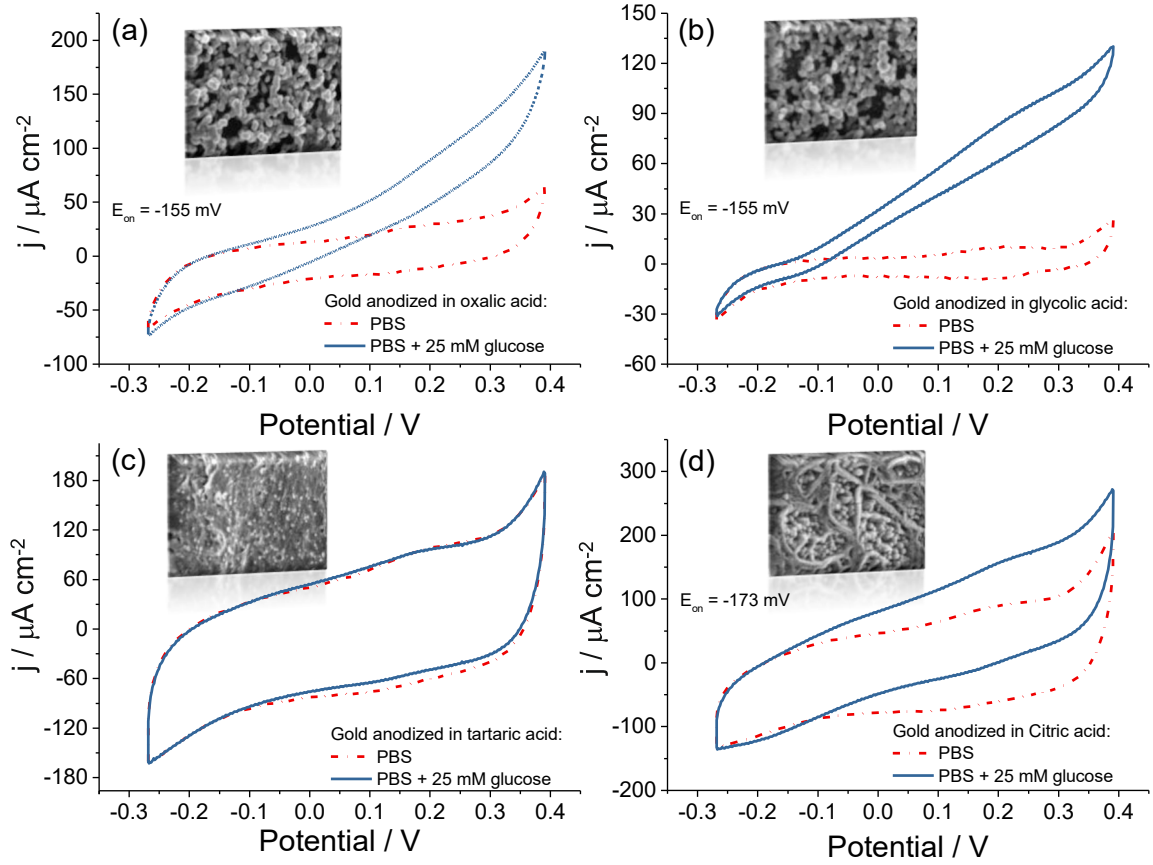

Fig. 4. Cyclic voltammograms of NPG/4-ATP/GDH bioanodes designed on the nanoporous gold electrode formed in oxalic (a), glycolic (b), tartaric (c) and citric (d) acids by one-pot anodization. All electrodes were operated in 0.1 M PBS (pH 7.4) in the presence (blue curve) and absence (red dotted curve) of 25 mM of glucose. Scan rate: 5 mV s^{-1}. Insets: SEM images of the particular NPG electrode surfaces.

compared to the case with NPG_{ox} (Fig. 3 b). Before the immobilization of GDH, the prepared electrodes were enriched with alkanethiol molecules. This modification provides a more optimally orientated enzyme, which is crucial for higher DET rates. Along with the high surface-to-volume ratio of NPG electrodes, the maximal electrocatalytic current output is possibly limited by only substrate diffusion and enzyme kinetics [33]. To form a self-assembly monolayer (SAM) on the NPG surfaces, the latter was soaked in a deoxygenated methanol solution containing 2 mM of 4-ATP for 2 h. Finally, after the immobilization of GDH, the DET-type bioelectrocatalytic activity of all NPG/4-ATP/GDH bioanodes was investigated by CV in the presence and absence of 25 mM of glucose (Fig. 4).

CV measurements evidenced that four-type NPG/4-ATP/GDH bioanodes exhibited no catalytic current in the absence of glucose (Fig. 4). After adding 25 mM glucose, the bioelectrocatalytic oxidation of glucose started at the onset potential (E_{on}) of −155 mV (in the case with NPG_{ox} and NPG_{gly}) and −173 mV (in the case with NPG_{cit} formed in citric acid). The maximal current densities (I-I_0) registered at 0.4 V were 125.4, 102.9 and 67.9 μA cm^{-2} for the bioanode based on NPG_{ox}, NPG_{gly} and NPG_{cit}, respectively (Fig. 4 a, b, d). In contrast, no bioelectrocatalytic current response was observed with bioanode based on NPG formed in tartaric acid (Fig. 4 c).

To confirm the DET coupling between the electrode and enzyme redox centre, NPG/GDH and the CNT-modified GC electrodes were utilized. As can be seen from CV analysis, the GC/CNT/GDH electrodes (without SAM) showed almost identical current densities towards glucose oxidation, thus evidencing DET-type bioelectrocatalysis (Fig S2 a). However, without 4-ATP, the NPG/GDH electrodes lost more than 60 % of their catalytic activity, proving that enzyme orientation plays a major role in developing powerful bioanodes.

Since the glucose oxidation onset potential was more negative (-155 mV) than the formal potential of 4-ATP molecules (217 mV), the latter cannot be assigned as a redox mediator and acted herein only by ensuring the proper enzyme orientation (Fig. S2 b). The electrochemical transformations of 4-ATP were described in detail in previous research [26]. Briefly, it is known that 4-ATP molecules can be oxidized at positive potentials by forming the 4-mercapto-N-phenylquinone diamine (MPQD), which is not stable enough in aqueous solutions and can be further hydrolysed to the 4-mercapto-N-phenylquinone monoamine (MPQM) (Fig. S3). These compounds are redox-active and can be identified during CV analysis. Furthermore, the surface-controlled redox waves observed at the higher potential sweep rates with the formal potential of −0.25 V (measured at 100 mV s^{-1}) suggesting that the redox centre of GDH enzyme possibly is membrane-bounded or at least are not deeply buried within the enzyme matrix (Fig. S2 c, d). The exact nature of the GDH co-factor has not yet been identified; however, according to the redox potential received, it might be ascribed to the heme-containing cytochromes. By comparing the obtained GDH performances on various types of NPG electrode and their rESA, it can be concluded that the chemical nature of NPG electrodes and surface morphology plays an essential role in developing enzymatic bioelectrodes on NPG surfaces. Since the rESA of NPG produced in tartaric acid is relatively high (74.4), the absence of bioelectrocatalytic current at first warned about the extremely low amount of immobilized enzyme. The possible explanation for such low surface coverage could be the presence of significant content of defects (i.e. step-edges) [33].

It was hypothesized that the tartaric acid molecules stabilized the defected sites and would remain adsorbed when soaked into the 4-ATP solution, thus less likely to exchange with free 4-ATP molecules. Moreover, to compare the electrocatalytic activity of various NPG electrodes, the CV curves were recorded in a 5 mM ferro/ferri redox couple containing 0.1 M PBS solution (pH = 7.4) at a scan rate of 100 mV s^{-1}. The results showed that the nanostructurization of gold electrodes increased the Faradaic current towards the redox processes of the Fe^{3+}/Fe^{2+} probe, confirming the higher surface area of electrodes (Fig. S4). The bare gold electrode's peak-to-peak separation (ΔE_p) was 91.7 mV. In contrast, the NPG electrodes showed slightly decreased ΔE_p values of 84.1, 77.9 and 87 mV, thus indicating higher reversibility and a bit faster electron transfer reactions (Table S1). However, in the case of the NPG electrode formed in tartaric acid, the $I_{p,c}$ and $I_{p,a}$ current values were more than ten fold lower than others, thus suggesting the poor electric conductivity of the electrode (Fig. S4). After the preliminary characterization of four types of NPG/4-ATP/GDH bioanodes, further studies focused on developing bioanodes based on NPG_{ox} and NPG_{gly}, whereas the highest bioelectrocatalytic performances were observed.

3.3. Anodization of bare gold in oxalic and glycolic acids

The blackening rate of gold *via* the anodization in oxalic and glycolic acids depends on various factors such as applied potential, reaction time, temperature, stirring conditions and electrolyte composition that plays an essential role in controlling the thickness and surface roughness of NPG films [23]. However, it was observed that applied potential and/or reaction time do not significantly change the surface morphology of NPG_{ox} and NPG_{gly} and mainly affect only the thickness of coatings. The impact of the concentration of glycolic acid on the NPG formation has also been tested herein by recording the gold reduction curves. It should be noted that the concentration does not affect the morphology of the NPG (data not shown). However, based on the results obtained (Fig. S5), it was revealed that the highest reduction current was observed when the gold was anodized in 1.8 M of glycolic acid solutions. This concentration was further used when anodized gold in glycolic acid.

The effect of applied potential (marked with black arrows in Fig. 5 a, d) on the formation of NPG with a fixed reaction period was tested as a function of rESA. The increased applied potential during the anodization of bare gold led to a significantly boosted gold reduction peak currents at 0.85–0.9 V (Fig. 5 b, e), thus resulting in an enhanced value of rESA as illustrated by histograms in Fig. 5 c and f. The rESA exhibited almost linear dependency on the applied potential ranging from 2 to 2.8 V and 3 to 6 V in the case of NPG_{ox} and NPG_{gly}, respectively. The highest rESA of 58.4 and 108.5can be achieved by controlling the applied potential when gold was anodized in oxalic and glycolic acids at 3.0 for 30 min and 6 V for 1 h, respectively. However, at the potential of 3.0 V, the rESA did not increase significantly compared to that obtained at 2.8 V, thus suggesting that the anodization of gold achieved the plateau stage. Contrarily, no saturation was observed with gold anodized in glycolic acid. Higher anodization voltages of > 3.2 V and > 6 V or even more extended anodization times caused the total collapse of NPG layers, consequently reducing rESA magnitudes, respectively. These findings matched those observed by Nishio et al. and further confirm that NPG mechanical strength decreased by increasing the porous layer thickness [25]. High electrode mechanical strength is mandatory for biosensors and biofuel cell applications and should be maintained. Here, it was found that the smoothest coatings of NPG with the higher mechanical stability could be produced in an optimized anodization condition: the anodization took place in gently stirred (150 rpm), 0.3 M oxalic and 1.8 M glycolic acids cooled to 4 °C at the potential ranging from 2.6 to 3.0 V and 3.8–5 V (vs. Ag/AgCl), for 30 and 60 min respectively.

The exact mechanism of NPG formation in oxalic acid remains unclear; however, some possible explanations related to the carbonaceous passivation of gold have been proposed to play an essential role in developing nanostructured surfaces [25]. To clarify the possible redox process occurring on the gold electrode, linear sweep voltammetry has been used (Fig. 5 a, d). The registered LSV curve obtained on bare gold surfaces in 0.3 M oxalic acid (Fig. 5 a) can be divided into a few distinct current regions. The first potential region from 0.7 to 1.5, whereas the anodic current starts to increase, reaches a plateau, and decreases, can be attributed to the formation of gold oxide layers [23] and irreversible oxidation of oxalic acid. In agreement with previous research [34], the latter process can be evidenced by comparing the magnitudes of anodic current observed during the CV analysis of bare gold in sulphuric and oxalic acids at 1.35 V, respectively (Fig. 5 b and Fig. 6 a).

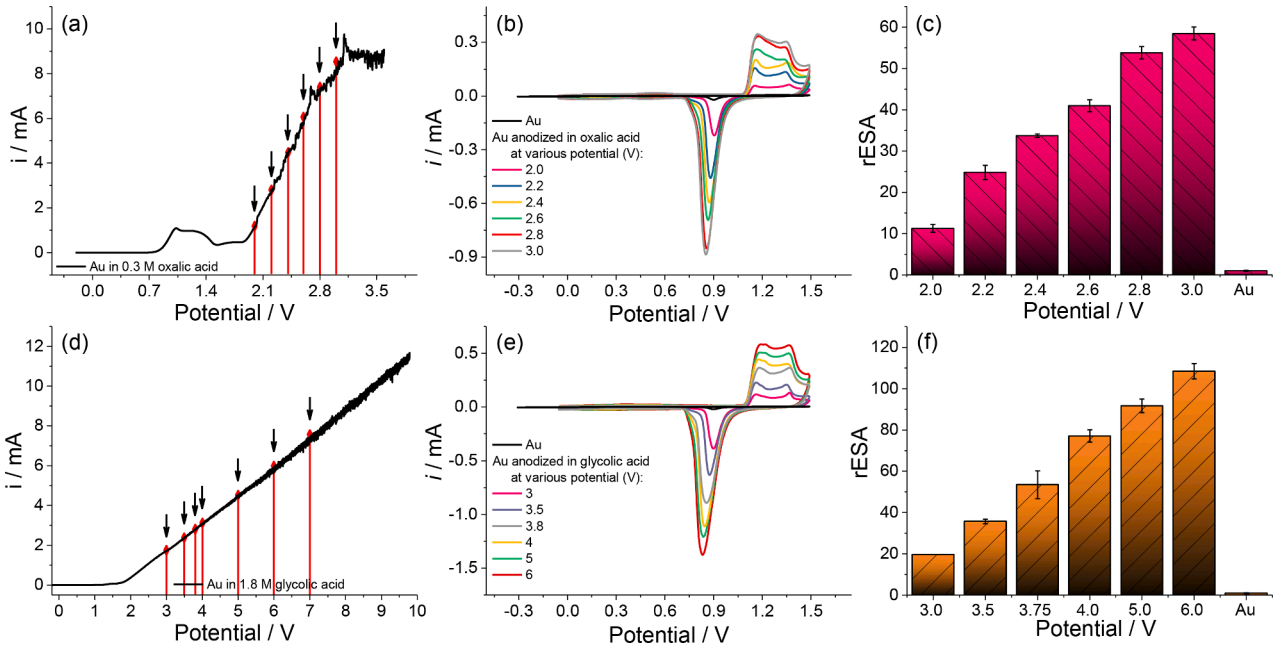

Fig. 5. Electrochemical characterization of bare gold and NPG electrodes. Linear sweep voltammogram of gold electrode recorded in 0.3 M oxalic (a) and 1.8 M glycolic (d) acid at 5 mV s^{-1}. The red lines and black arrows indicate the potential values selected for anodization. Cyclic voltammograms of NPG electrodes anodized for 0.5 and 1.0 h in oxalic (b) and glycolic (e) acid solutions at the different applied potentials. All CV curves were registered in 0.1 M H_2SO_4 at 50 mV s^{-1}. Histograms (c, f) show the relative (normalized with respect to bare gold) electrochemical surface area (rESA) of NPG electrodes formed in oxalic (c) and glycolic (f) acids.

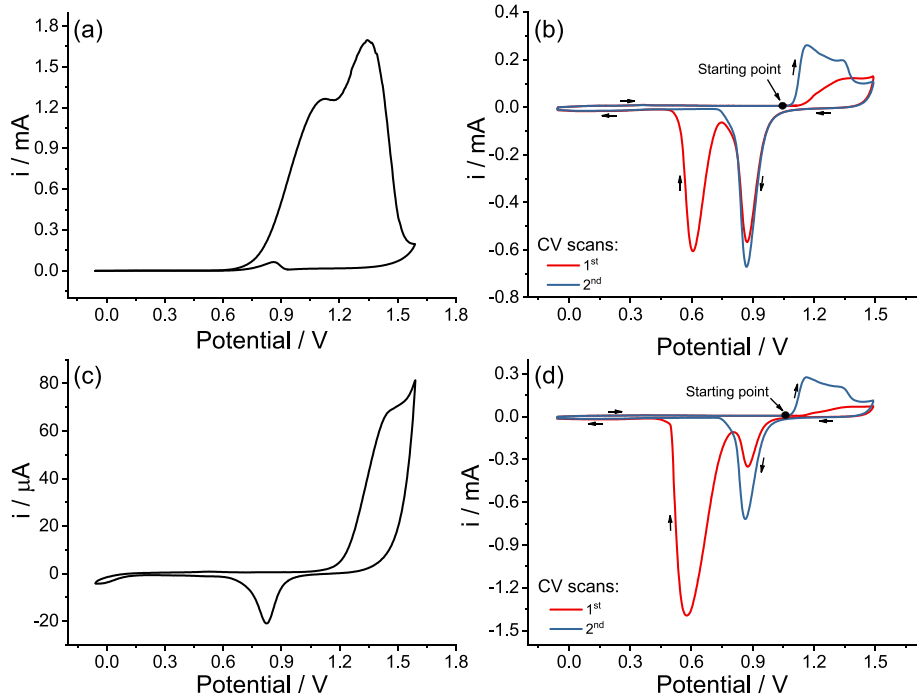

Fig. 6. CV of a bare gold electrode in 0.3 M oxalic (a) and 1.8 M glycolic (c) acids. CV of as-prepared NPG electrodes after anodization in oxalic (b) and glycolic (d) acids. Curves (b, d) were recorded in 0.1 M sulphuric acid solutions at 50 mV s^{-1} under quiescent conditions.

The magnitude of anodic current of bare gold oxidation in 0.5 M H_2SO_4 was more than two orders of magnitude lower compared to that observed in 0.3 M oxalic acid, proving that the oxidation of oxalic acid occurs on the bare gold at higher rates with the onset potential of 0.54 V. Additionally, no typical gold reduction peak at ~ 0.9 V was observed in CV traces, evidencing the absence of gold oxide (Fig. 6 a). The second potential region from 1.5 to 1.85 V with the anodic current drop results in gold passivation by gold oxides [23]. The third potential region investigated herein was from 1.85 to 3.5 V, where the oxygen evolution reaction (OER) occurs. It is important to note that the blackening of bare gold electrodes was successfully achieved only at this potential range.

The electrochemical behaviour of bare gold electrodes in glycolic acid completely differs from that observed in oxalic acid and exhibits a significant current increase only due to OER, which starts at the onset potential of 1.6 V (Fig. 5 d). The control experiments evidenced that gold oxide formation occurred at a higher rate than in the case with oxalic

acid; consequently, the reduction peak at 0.82 V was observed (Fig. 6 c). The $E_{p,c}$ was slightly shifted to a negative direction compared to typical gold reduction ($E_{p,c} \approx 0.9$ V); however, it might be explained by the higher glycolic acid solution (pH ≈ 1.6).

Although the NPG formation was done without the assistance of Cl^- ions herein, as-grown NPG layers showed similar behaviour in terms of temporary gold oxide layer formation, which is a prerequisite for verification of the mechanism of anodic production of NPG described in [35]. To prove this, as-prepared NPG_{ox} and NPG_{gly} electrodes were submerged into the 0.5 M H_2SO_4 solution, and the CV curves were registered. As shown from Fig. 6 b and d, in the first cathodic scan, two large reduction peaks with the $E_{p,c}$ values of 0.60 V and 0.87 V (NPG_{ox}); 0.58 and 0.87 V (NPG_{gly}) were observed, respectively. Both reduction peaks might be attributed to the reduction of gold oxides (Au^{3+}) such as Au_2O_3, AuOOH, $Au(OH)_3$ or their non-stoichiometric compounds. Similar results were observed in a previous study, which showed that NPG fabricated by the anodization of gold in KCl solutions exhibits almost the same electrochemical properties [23]. However, in both cases, the reduction peaks at the lower potentials completely disappeared after the first scan. Furthermore, the anodic current of gold oxide formation implies that the NPG surface is not fully oxidized after the anodization in oxalic and glycolic acids. However, the current shape and gold oxidation onset potentials indicate clear differences between the first and second CV scans (Fig. 6 b and d). The higher onset potentials and lower oxidative current illustrate that the NPG surface is affected by adsorbed carboxylic acids that suppress the gold oxide formation by adsorbed carboxylates. Similar effects of carboxylic acid adsorption on gold at relatively high anodic potentials were observed by Paik et al. [36]. According to the proposed possible mechanisms of the NPG layers formation in Cl^- containing electrolytes and obtained results, it might be predicted that NPG production in oxalic and glycolic acids follows comparable pathways through the gold dissolution and re-deposition mechanism [17,23]. Based on the results presented in this study, we hypothesised that the NPG_{ox} growth starts with forming a gold oxide (Au^{3+}) layer. The subsequent breakdown of the oxide film possibly led to the development of nanopores on a gold anode. When deep (enough) pores are obtained, the top layers might be reduced to gold by oxalate (or its ionic species), possibly with the assistance of O^{2-} (or other oxygen-containing species). Carbonaceous species might further passivate the reduced layers, as hypothesized in a previous study [25]. Since the blackening of gold was only achieved with oxalic acid, we predict these changes should be related to the oxalate molecule structure and its specific interactions with gold and other ionic species in solution. The high catalytic current densities of oxalic acid oxidation imply that its electrooxidation (on gold electrode) occurs faster than all other organic acids tested in this study. It should be noted that this phenomenon is specific to the oxalic acid and not to the metal chosen since a similar behaviour was demonstrated on the platinum electrode (data not shown). However, more profound studies are required to clarify the NPG formation mechanism in organic acid electrolytes.

3.4. XPS analysis of NPG electrodes

Since the presence of gold oxide on the surface of NPG_{ox} and NPG_{gly} was evidenced by CV analysis, a more precise analysis was used to clarify the chemical states of the elements in NPG nanostructures. To examine the chemical properties of the NPG_{ox} and NPG_{gly} electrode, the X-ray photoelectron spectroscopy (XPS) analysis was performed herein. The survey spectra of "as-prepared" NPG_{ox} and NPG_{gly} coatings reflected the presence of Au, O and C elements (Fig. S6 and S7 a). The XPS spectra in the regions of Au 4f, O1s and C1s and their depth profiles after Ar^+ ion sputtering for 0 to 240 s are presented in Fig. 7, Fig. S6 and S7, respectively. In the case of NPG_{gly}, the deconvolution of Au 4f spectra showed three $4f_{7/2}$ and $4f_{5/2}$ peaks at BE of 84.5, 84.9 and 86.6 eV, which corresponds to the photoelectrons emitted from metallic gold (Au^0) and Au^{+3} species, most likely related to the presence of Au_2O_3 and $Au(OH)_3$, respectively (Fig. 7 a) [37,39,40]. The binding energy shift to a higher energy direction by a value of 0.5 eV compared with pure gold (BE = 84 eV) illustrates that the chemical state of gold is affected by the nature of different carboxylate molecules originating from the NPG formation process. The fitting of the O 1s region indicates four prominent peaks that appeared at 530.5, 531.4, 532.4 and 533.6 eV. The peak at 532.4 eV can be prescribed to the adsorbed organic C-O bonds, whereas the two peaks at 530.5 and 531.4 eV, represent the Au^{+3} state in Au_2O_3 and $Au(OH)_3$ species, respectively (Fig. 7 b) [40,41]. Furthermore, the deconvolution of the C 1s region gave four peaks at 284.9, 286.6, 288 and 288.9 eV that may be assigned to the typical C–C or C–H, C-OH, C = O and COOH bonds, respectively (Fig. 7 c) [38]. In order to

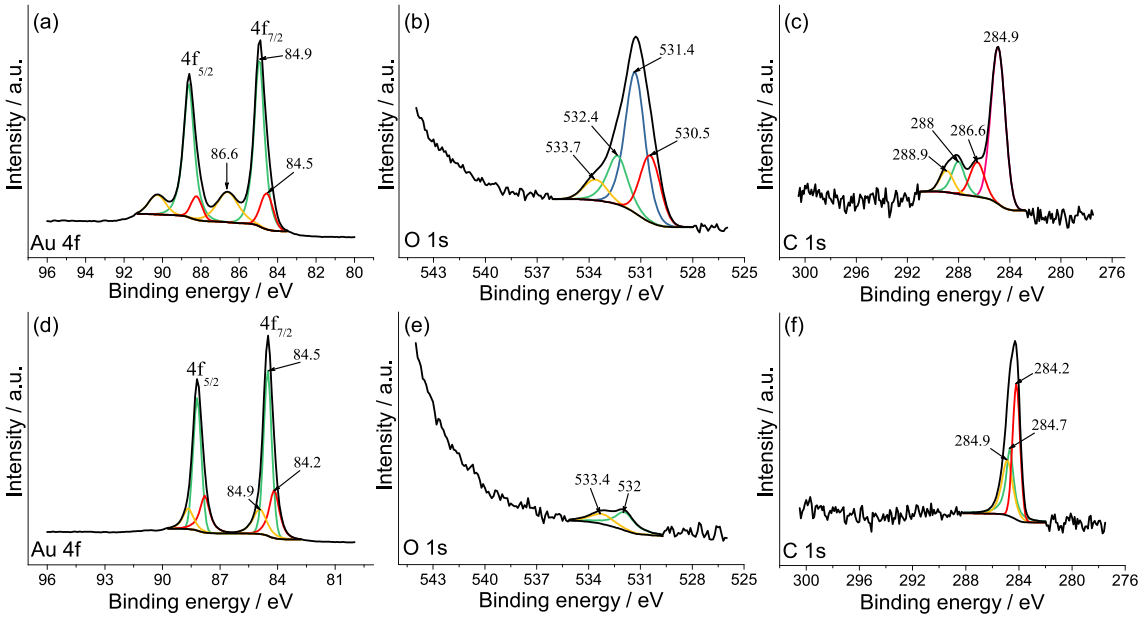

Fig. 7. High-resolution deconvoluted X-ray photoelectron spectra of Au 4f (a,d), O1s (b,e) and C 1s (c, f) of as-prepared NPG electrode fabricated *via* anodization of bare gold in 1.8 M glycolic (top row) and 0.3 M oxalic acids (bottom row), respectively. The XPS analysis was carried out immediately after the anodization of bare gold.

evidence the oxygen-containing gold compound's co-existence in the deeper layers of NPG, the depth profiling XPS analysis has been performed. As can be seen from Table S2, in the case of NPG_{gly}, the content of carbon disappeared after the first step of Ar^+ ion sputtering, whereas the amount of oxygen gradually decreased after each stage and remained detectable even after 270 s of exposure to Ar^+ (1.2, at. %). These results match well those obtained *via* electrochemical analysis and indicate that the "as-grown" NPG_{gly} surface is covered with protective oxygen-containing gold composites, most likely attributed to Au_2O_3 and $Au(OH)_3$ as observed in previous research [23,41]. In contrast to NPG_{gly} layers, the NPG_{ox} surfaces exhibited only traces of Au_2O_3, as shown by the peak that appeared at the BE = 84.9 eV in the Au 4f (Fig. 7 d).

The core-level spectra of O 1s orbital resulted in two low-intensity peaks at 532.0 and 533.4 eV, which can be assigned to the water and possibly surface-adsorbed species (Fig. 7 e). It should be noted that no apparent peak in the 530–532 eV region was registered, thus revealing that NPGox layers contain metallic gold (Au0) and agree with the previous pioneered research [25]. Interestingly, the deconvolution of the C 1s region showed three peaks at BE = 284.9, 284.2 and 284.7 eV, which can be attributed to the photoelectrons emitted from C-C and C–H bonds (Fig. 7 f). No peaks at higher BE values were observed (286–289 eV), whereas the oxygen-containing functional groups should be located. From this observation, it can be hypothesized that oxalic acid adsorption on NPG was less favourable than glycolic acid. On the other hand, it might withdraw from the NPG surface more quickly than glycolic acid after thoroughly rinsing with distilled water. Furthermore, after 30 s of the Ar^+ ion sputtering, the carbon and oxygen-based contaminations disappeared (Table S2), suggesting the presence of pure gold in the NPG_{ox} layer.

3.5. Impact of DET performance on the anodization potential of bare gold

Since the considerable redox reactions occur mainly on the external sites of the NPG, the bioanode performances depend on the amount of specifically-orientated enzyme immobilization on the top layers of nanostructured gold. It was observed that NPG structures could accelerate the electron transfer between the enzyme's redox centre and solid electrodes and, in some cases, facilitate the orientation of the enzymes into the DET-capable position, leading to higher bioelectrocatalytic responses as recently displayed with laccase and horseradish peroxidase enzymes [34,42]. Nevertheless, the amount of orientated enzymes deeply buried into the pores (adsorbed on the bottom part of pores) does not significantly impact the bioelectrode efficiency because of substrate diffusion limitations within the porous gold nanostructures. From this point, it is logical to note that the thick layers of NPG are not required for a robust bioelectrode. However, the top few layers of NPG must exhibit a uniform morphology and minimal mechanical resistance, which decreased after the high applied voltage regime and prolonged anodization. To gain more information about the impact of NPG/4-ATP/GDH bioanode's performance on the anodization regime, the different applied potential was used to produce the NPG_{ox} and NPG_{gly}. In the case of bioanodes designed on NPG_{ox}, the higher bioelectrocatalytic current densities of 230.7 μA cm^{-2} were achieved when gold was anodized at 2.8 V (Fig. 8 a, b). When the gold electrode was anodized at the potential gap ranging from 2.4 to 3.0 V, the obtained current densities of NPG/4-ATP/GDH bioanode in the presence of 25 mM glucose would exhibit the

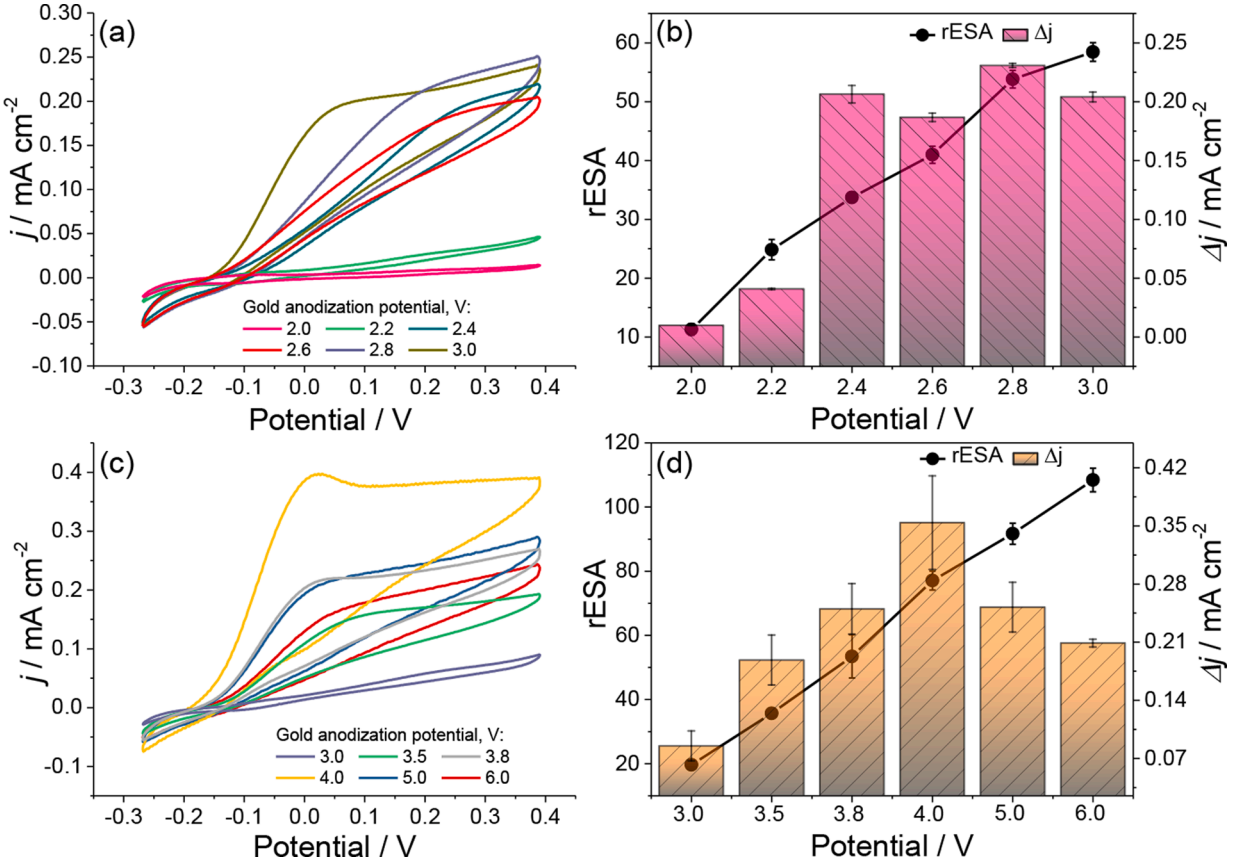

Fig. 8. The GDH-based bioanodes performance dependency on the different applied potential during the anodization of bare gold electrodes in 0.3 M oxalic (top row) and 1.8 M glycolic (bottom row) acids for 30 and 60 min, respectively. CVs of NPG/4-ATP/GDH bioanodes designed on the NPG electrode produced at different applied potential regimes. All electrodes were operated in 0.1 M PBS (pH 7.4) in the presence of 25 mM of glucose. Scan rate: 5 mV s^{-1}. Histograms (b, d) show the relative (normalized with respect to bare gold) electrochemical surface area (rESA) of NPG electrodes and the GDH-based bioanode performance dependency on the applied potential for NPG production.

comparable values of 187–231 μA cm^{-2}. Taking into account that rESA increased almost linearly towards all applied potential regions, proving the porous structure formation and higher surface area of NPG evolution, the providing bioelectrocatalytic current densities of NPG/4-ATP/GDH bioanodes supports the above-highlighted statement about the cover layers of NPG importance rather than deep porous structures for bioelectrocatalysis (Fig. 8 b).

These results match well those obtained from CV analysis of NPG_{ox} structures, whereas the waves of $[Fe(CN)_6]^{4-/3-}$ redox couple that possess fast heterogeneous electron transfer kinetics [33] was slightly more intense than a bare gold electrode, suggesting that the planar diffusion of redox species dominated (Fig. S4). In the NPG_{gly}-based bioanodes, the bioelectrocatalytic current density increased linearly, respecting the rESA and applying anodization potential ranging from 3 to 4 V (Fig. 8 c, d). The highest value of 354 μA cm^{-2} was obtained with an NPG electrode formed *via* the anodization of gold at 4.0 V in the presence of 25 mM glucose. Furthermore, the optimized anodization voltages vary between 3.8 and 5.0 V, whereas the current densities ranged from 250 to 354 μA cm^{-2}. The maximal bioelectrocatalytic current of NPG/4-ATP/GDH bioanode based on NPG_{gly} was at least 35 % higher than NPG_{ox}, while the apparent Michaelis constant of 5.6 and 6.0 mM was estimated (Fig. S8), evidencing that nanoporous gold surfaces formed by anodization in glycolic acid are more suitable for the bioelectrochemical applications. This phenomenon could be explained due to a few possible reasons that are related to the behaviour of NPG [21]: firstly, the NPG_{gly} layer is composed of almost 20 nm smallest nanoparticles, thus providing a higher surface area suitable for enzyme immobilization as shown by higher rESA values; since the NPG_{gly} layers are comprised of oxygen-containing compounds most-likely attributed to $Au(OH)_3$ and Au_2O_3, as proved by HR-XPS analysis, it was assumed that NPG_{gly} layers could have more defective sites and lattice strains, resulting into the enhanced stability of self-assembly monolayers as have been discovered by Hakamada et al. [41]; since the pore diameter in NPG_{gly} is 16 nm smaller than NPG_{ox} (as illustrated by SEM analysis), the enzyme that is confined within the nanoporous gold structures exhibit higher stability. This feature was also shown in current research, whereas the NPG/4-ATP/GDH bioanode stability was tested *via* CV by measuring the current densities at 0.4 V in the presence of 25 mM glucose. The results indicated that the NPG_{gly}-based bioanode exhibited superior long-life operating stability towards glucose oxidation over 21 days by losing 23.9 % of its initial bioelectrocatalytic activity (Fig. S9 b). In contrast, the NPG_{ox}-based bioanode current densities dramatically decreased over the 12 days of measurements and lost almost 89.8 % of its activity (Fig. S9 a). It should be noted that all enzymatic electrodes were prepared by extending the immobilization time of 4-ATP molecules from 2 h to 14 h (except those described in section 3.1) since the higher glucose oxidation current magnitudes of 231 and 354 μA cm^{-2} and lower on set potentials of −183 and −175 mV (vs Ag/AgCl) have been registered for NPG_{ox} and NPG_{gly}-based bioanodes, respectively. The higher bioelectrocatalytic current values and lower glucose oxidation onset potentials suggest that prolonged time for SAM's immobilization facilitates DET rates and reduces the overpotential drop compared to the reduction potential of −0.45 V vs SHE for glucose/gluconolactone redox couple as estimated at pH = 7 and high substrate concentrations [42].

3.6. *The performance of mediator-less glucose bioanode*

The performance of mediator-less NPG/4-ATP/GDH bioanode constructed on various NPG_{ox} and NPG_{gly} electrodes has been estimated by using an H-type cell and two-electrode configuration, whereas the Pt sheet was submerged into the 0.1 M PBS containing 20 mM of $[Fe(CN)_6]^{3-}$ separated from bioanode by Nafion 115 proton exchange membrane (PEM) and acted as a cathode. The power density generated by the bioelectrodes was calculated from the polarization curves acquired in the presence of 25 mM glucose (Fig. 9 b, e). The obtained result agreed with the data from CV analysis, whereas the higher bioelectrocatalytic glucose oxidation current at 0.4 V was registered with the bioanodes designed on NPG_{ox} and NPG_{gly} electrodes formed at the potential of 2.8 and 4.0 V, respectively. The maximal power density (P_{max}) of bioanode based on NPG_{ox} electrode was found to be 2.3 fold lower compared to NPG_{gly}-based bioanode (Fig. 9 a, d). These power outputs achieved the magnitude of 14.0 and 31.8 μW cm^{-2} obtained at

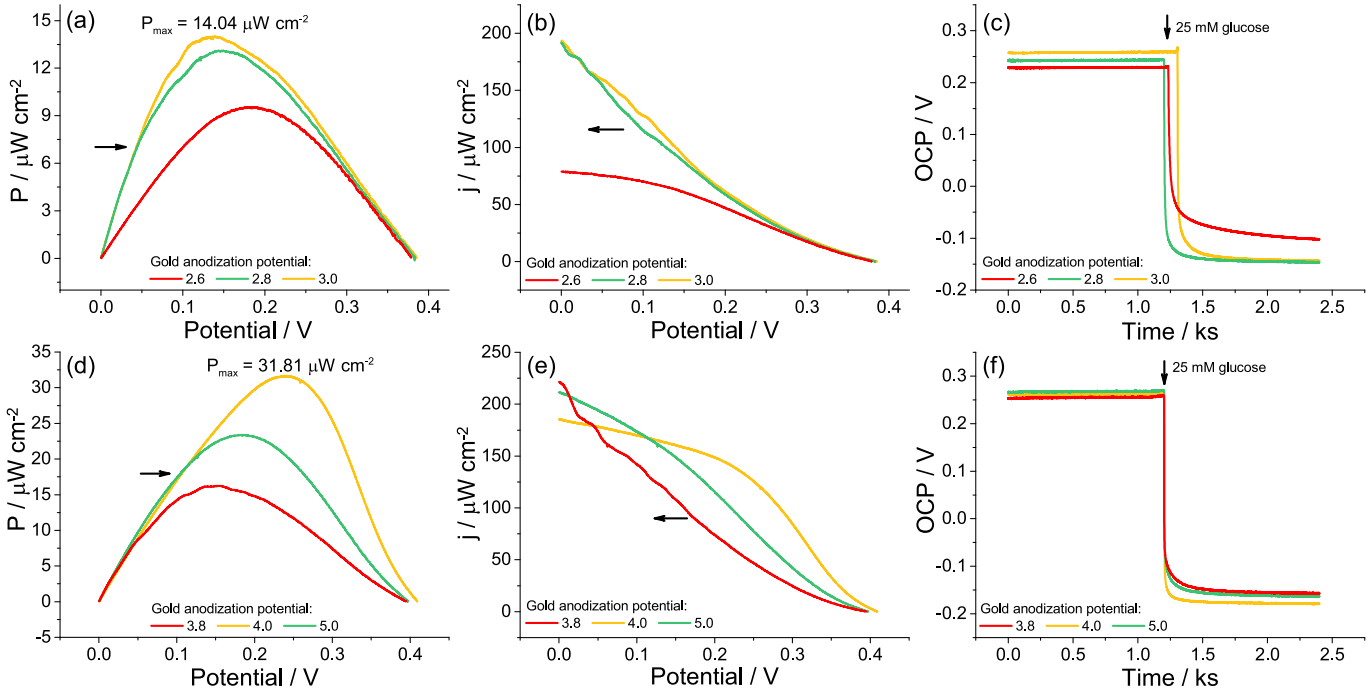

Fig. 9. Power density (a, d), polarization curves (b, e) and open-circuit potential (c, f) evolution of bioanodes comprised of GDH from *E. americana* immobilized on NPG electrode electrochemically-formed in 0.3 M oxalic (a-c) and 1.8 M glycolic (d-f) acids, respectively. The polarization curves were recorded in an H-type cell separated by a Nafion 115 membrane. All bioanodes were operated in 0.1 M PBS (pH 7.4) in the presence of 25 mM of glucose. Scan rate: 125 μV s^{-1}.

the potential of 140 and 240 mV, respectively. The received power outputs are relatively high and are in accordance with the previous research on glucose-powered bioanodes (Table S4). Besides, the superior DET and excellent biocatalytic activity of various NPG/4-ATP/GDH bioanodes were indicated by tracking a particular electrode's open circuit potential (OCP). The initial OCP of all tested bioanodes varies from 230 to 270 mV. After adding 25 mM glucose, the OCP rapidly decreased, reaching a stable magnitude between −101 and −179 mV (Fig. 9 c, e). Furthermore, the higher OCP differences of 402 and 441 mV correlated to the power outputs and CV results, proving that the most powerful bioanodes were designed on the NPG electrodes formed *via* the anodization of bare gold in oxalic and glycolic acids at 2.8 and 4.0 V, respectively.

The NPG coatings, especially formed *via* the chemical or electrochemical dealloying approach, have been widely used to develop non-enzymatic glucose sensors [16]. Since the bare NPG surface can oxidize glucose at the metal/solution interface in the presence of molecular oxygen, as shown by CV analysis (Fig. 10 a), the possible interference reactions that occur spontaneously on the electrode at the tested potential ranges have to be investigated. The electrochemical glucose oxidation occurred at NPG electrodes with the onset potential of −40 mV and reached the maximal current densities of 117 μW cm^{-2} at 0.25 V. However, after immobilising bovine serum albumin (BSA) on the NPG/4-ATP electrodes, the glucose oxidation rate became negligible (Fig. 10 b). The analogous results were observed by tracking the OCP of NPG and NPG/4-ATP/BSA electrodes. It was found that after the immobilization of non-conducive BSA, the OCP decreased gradually and completely differed from a bare NPG, whereas a sudden reduction in OCP occurred after adding 25 mM glucose (Fig. 10 c).

The slow reduction of electrode OCP, as well as the decrease in bioelectrocatalytic current, can be attributed to the metallic surface "contamination" by proteins that tend to inhibit the catalytic properties of NPG, as evidenced in our previous research, whereas the catalytic acceleration of enzymes on gold nanoparticles have been extensively revised [43]. These results indicate that the determined magnitude of bioelectrocatalytic current and power outputs of NPG/4-ATP/GDH-based bioanodes can be referred to as the DET bioelectrocatalysis of GDH on the NPG electrodes.

Since the NPG_{gly} layers contain Au_2O_3 and $Au(OH)_3$, as proved by XPS analysis, it was assumed that these factors could influence the charge transfer properties of the whole bioanode. To clarify this issue, the heterogeneous electron transfer constant k_0 was determined for bare, NPG_{ox} and NPG_{gly} electrodes using the $[Fe(CN)_6]^{3-/4-}$ electroactive redox probe. The estimated k^0, 8.5×10^{-4} cm s^{-1} for the bare gold electrode is relatively slow, whereas the NPG_{ox} and NPG_{gly} exhibited the enhanced values of 2.9×10^{-3} and 3.3×10^{-3} cm s^{-1}, respectively (Table S3). The peak currents ($i_{pa,c}$) estimated with bare gold, NPG_{gly} and NPG_{ox} electrodes increase linearly with the square root of the scan rate, indicating the diffusion-controlled process (Fig. S10). However, the peak-to-peak separations provided in Table S3 possessed quasi-reversible responses influenced by heterogeneous electron transfer dynamics and diffusion control [44]. To realize a deeper insight into the effects of nanostructurization of bare gold electrodes *via* anodization, electrochemical impedance spectroscopy (EIS) measurements were performed herein. It was found that the solution resistance for all tested electrodes varied from 3.5 to 4.5 Ω cm^2 and did not significantly depend on the electrode composition (Fig. S11 insets). However, the charge transfer resistance of the bare gold electrode was at least ten fold higher than both NPG electrodes and reached an approximated magnitude of 5.5 Ω cm^2 (Fig. S11). By their substantially increased rESA and accelerated electron transfer rate, such NPG electrodes could be suitable for developing a porous transducer layer for biosensors and biofuel cell design.

4. Conclusions

This work aimed to bring new insights into the current nanoporous gold surface production knowledge *via* one-step anodization of planar gold electrodes in organic acid solutions and its adaptation and optimization for bioanode construction. We have shown that anodization of bare gold electrodes in oxalic, glycolic, tartaric and citric acid significantly enhances the surface area of electrodes by producing thin porous films with entirely different morphology. The NPG_{ox} and NPG_{gly} layers comprised of oval and round-shaped nanoparticles with an averaged diameter of 38.2 and 20.1 nm, respectively, have been extensively investigated as transducer layers for GDH-based bioanode design. We have shown that NPG_{ox} consists of pure metallic gold (Au^0), whereas the NPG_{gly} layers have a significant quantity of $Au(OH)_3$ and Au_2O_3 compounds. The diffusion-controlled process's heterogeneous electron transfer constant k^0 was estimated for NPG and bare gold electrodes, providing 3.4 and 3.8-fold higher rates for both NPG electrodes. Furthermore, EIS analysis suggested that both NPGs reduce the charge transfer resistance at least ten fold compared to a planar gold electrode, thus providing a suitable environment for enzyme action. Besides, we found that the most effective DET-type performances of NPG/4-ATP/GDH bioanode were achieved when the gold was anodized in oxalic and glycolic acids at the potential gaps ranging from 2.4 to 3.0 V and from 3.0 to 4.0 V, respectively. The maximal bioelectrocatalytic current density towards glucose oxidation was received with bioanodes based on NPG_{ox} and NPG_{gly} electrodes reaching the values of 231 and 354 μA cm^{-2} in the presence of 25 mM glucose at 0.4 V. The power density measurements show comparable results, whereas the P_{max} 14.0 and 31.8 μW cm^{-2} magnitudes were estimated for NPG_{ox} and NPG_{gly}-based bioanodes. Furthermore, the NPG_{gly}-based bioanode possessed considerably higher long-life stability by losing 23.9 % of its catalytic activity after 21 days. In contrast, the NPG_{ox}-based bioanode lost almost 89.8 % of its activity even after 12 days. To conclude, we have noted that considerably higher bioelectrocatalytic performances of the bioanode

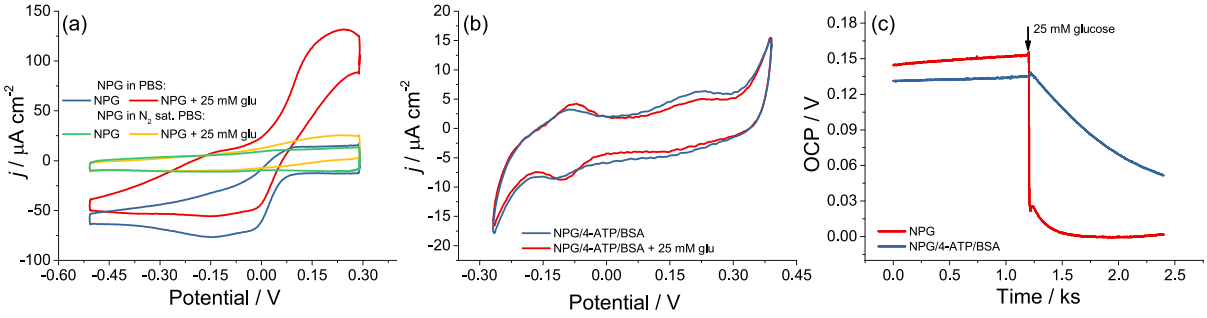

Fig. 10. (a) CVs of bare NPG electrode (formed in glycolic acid) in the presence (red and yellow curves) and absence (blue and green curves) of 25 mM of glucose. (b) CVs of NPG/4-ATP/BSA electrodes in the presence (red curve) and absence (blue curve) of 25 mM of glucose. (c) Open circuit potential variations of bare NPG (red dotted curve) and NPG/4-ATP/BSA (blue dotted curve) electrodes before and after the addition of 25 mM glucose. All electrodes were operated in 0.1 M PBS (pH 7.4) under quiescent conditions at a scan rate of 5 mV s^{-1}.

based on NPG_{gly} were primarily achieved due to a few possible reasons: (*i*) almost 20 nm reduced particles size increased the surface area thus resulting in the higher content of immobilized enzyme; (*ii*) higher stability of NPG_{gly} layers; (*iii*) enhanced stability of SAM results to improved electron transfer between the porous electrode and enzyme. We believe this technology can be applied on various gold surfaces, i.e., as screen-printed electrodes providing significantly enhanced surface area and allowing us to avoid the nanostructurization by a painful gold-NPs drop-casting path, thus being more convenient for usage as a main transducer layer for any of biorecognition element immobilization.

CRediT authorship contribution statement

Rokas Žalnėravičius: Formal analysis, Methodology, Data curation, Visualization, Writing – original draft, Writing – review & editing. **Arnas Naujokaitis:** Formal analysis, Writing – review & editing. **Vitalija Jasulaitienė:** Methodology, Formal analysis, Writing – review & editing. **Rasa Rutkienė:** Methodology, Resources, Writing – review & editing. **Rolandas Meškys:** Methodology, Resources, Writing – review & editing. **Marius Dagys:** Conceptualization, Supervision, Funding acquisition, Writing – review & editing.

Declaration of Competing Interest

The authors declare that they have no known competing financial interests or personal relationships that could have appeared to influence the work reported in this paper.

Data availability

Data will be made available on request.

Acknowledgements

This project has received funding from the Research Council of Lithuania (LMTLT), agreement No P-PD-22-079. We are grateful to dr. Tadas Ragaliauskas for the sputtered gold specimens.

Appendix A. Supplementary data

Supplementary data to this article can be found online at https://doi.org/10.1016/j.apsusc.2023.158654.

References

[1] R.A.S. Luz, A.R. Pereira, J.C.P. de Souza, F.C.P.F. Sales, F.N. Crespilho, Enzyme biofuel cells: thermodynamics, kinetics and challenges in applicability, ChemElectroChem 1 (2014) 1751–1777, https://doi.org/10.1002/celc.201402141.

[2] S. Yu, N.V. Myung, Recent advances in the direct electron transfer-enabled enzymatic fuel cells, Front. Chem. 8 (2021), 620153, https://doi.org/10.3389/fchem.2020.620153.

[3] F. Tasca, L. Gorton, W. Harreither, D. Haltrich, R. Ludwig, G. Nöll, Comparison of direct and mediated electron transfer for cellobiose dehydrogenase from *Phanerochaete sordida*, Anal. Chem. 81 (2009) 2791–2798, https://doi.org/10.1021/ac900225z.

[4] I. Mazurenko, X. Wang, A. de Poulpiquet, E. Lojou, H_2/O_2 enzymatic fuel cells: from proof-of-concept to powerful devices, Sustain. Energy Fuels. 1 (2017) 1475–1501, https://doi.org/10.1039/C7SE00180K.

[5] T. Ruzgas, Enzyme-based (bio)fuel cells-bilirubin oxidase use, Oxford, Elsevier (2018) 209–216, https://doi.org/10.1016/B978-0-12-409547-2.13587-5.

[6] S. Shleev, V. Andoralov, D. Pankratov, M. Falk, O. Aleksejeva, Z. Blum, Oxygen electroreduction versus bioelectroreduction: direct electron transfer approach, Electroanalysis 28 (2016) 2270–2287, https://doi.org/10.1002/elan.201600280.

[7] M.T. Meredith, S.D. Minteer, Biofuel cells: enhanced enzymatic bioelectrocatalysis, Annu. Rev. Anal. Chem. 5 (2012) 157–179, https://doi.org/10.1146/annurev-anchem-062011-143049.

[8] O. Smutok, T. Kavetskyy, E. Katz, Recent trends in enzyme engineering aiming to improve bioelectrocatalysis proceeding with direct electron transfer, Curr. Opin. Electrochem. 31 (2022), 100856, https://doi.org/10.1016/j.coelec.2021.100856.

[9] H. Chen, O. Simoska, K. Lim, M. Grattieri, M. Yuan, F. Dong, Y.S. Lee, K. Beaver, S. Weliwatte, E.M. Gaffney, S.D. Minteer, Fundamentals, applications, and future directions of bioelectrocatalysis, Chem. Rev. 120 (2020) 12903–12993, https://doi.org/10.1021/acs.chemrev.0c00472.

[10] N.R. Mohamad, N.H.C. Marzuki, N.A. Buang, F. Huyop, R.A. Wahab, An overview of technologies for immobilization of enzymes and surface analysis techniques for immobilized enzymes, Biotechnol. Biotechnol. Equip. 29 (2015) 205–220, https://doi.org/10.1080/13102818.2015.1008192.

[11] Y. Gao, Y. Zhou, R. Chandrawati, Metal and metal oxide nanoparticles to enhance the performance of enzyme-linked immunosorbent assay (ELISA), ACS Appl. Nano Mater. 3 (2020) 1–21, https://doi.org/10.1021/acsanm.9b02003.

[12] D. Ratautas, L. Marcinkevičienė, R. Meškys, J. Kulys, Mediatorless electron transfer in glucose dehydrogenase/laccase system adsorbed on carbon nanotubes, Electrochim. Acta 174 (2015) 940–944, https://doi.org/10.1016/j.electacta.2015.06.063.

[13] A. Ramanavičius, A. Ramanavičienė, A. Malinauskas, Electrochemical sensors based on conducting polymer-polypyrrole, Electrochim. Acta 51 (2006) 6025–6037, https://doi.org/10.1016/j.electacta.2005.11.052.

[14] I. Mazurenko, K. Monsalve, P. Infossi, M.T. Giudici-Orticoni, F. Topin, N. Mano, E. Lojou, Impact of substrate diffusion and enzyme distribution in 3D-porous electrodes: a combined electrochemical and modelling study of a thermostable H_2/O_2 enzymatic fuel cell, Energ. Environ. Sci. 10 (2017) 1966–1982, https://doi.org/10.1039/C7EE01830D.

[15] P. Bollella, Y. Hibino, K. Kano, L. Gorton, R. Antiochia, Highly sensitive membraneless fructose biosensor based on fructose dehydrogenase immobilized onto aryl thiol modified highly porous gold electrode: characterization and application in food samples, Anal. Chem. 90 (2018) 12131–12136, https://doi.org/10.1021/acs.analchem.8b03093.

[16] Y. Xia, W. Huang, J. Zheng, Z. Niu, Z. Li, Nonenzymatic amperometric response of glucose on a nanoporous gold film electrode fabricated by a rapid and simple electrochemical method, Biosens. Bioelectron. 26 (2011) 3555–3561, https://doi.org/10.1016/j.bios.2011.01.044.

[17] Y. Mie, H. Takayama, Y. Hirano, Facile control of surface crystallographic orientation of anodized nanoporous gold catalyst and its application for highly efficient hydrogen evolution reaction, J. Catal. 389 (2020) 476–482, https://doi.org/10.1016/j.jcat.2020.06.023.

[18] M.N. Hossain, Z. Liu, J. Wen, A. Chen, Enhanced catalytic activity of nanoporous Au for the efficient electrochemical reduction of carbon dioxide, Appl. Catal. B Environ. 236 (2018) 483–489, https://doi.org/10.1016/j.apcatb.2018.05.053.

[19] R. Zeis, T. Lei, K. Sieradzki, J. Snyder, J. Erlebacher, Catalytic reduction of oxygen and hydrogen peroxide by nanoporous gold, J. Catal. 253 (2008) 132–138, https://doi.org/10.1016/j.jcat.2007.10.017.

[20] Y. Takahashi, M. Wanibuchi, Y. Kitazumi, O. Shirai, K. Kano, Improved direct electron transfer-type bioelectrocatalysis of bilirubin oxidase using porous gold electrodes, J. Electroanal. Chem. 843 (2019) 47–53, https://doi.org/10.1016/j.jelechem.2019.05.007.

[21] P. Bollella, Porous gold: a new frontier for enzyme-based electrodes, Nanomaterials 10 (2020) 722, https://doi.org/10.3390/nano10040722.

[22] T. Adachi, T. Fujii, M. Honda, Y. Kitazumi, O. Shirai, K. Kano, Direct electron transfer-type bioelectrocatalysis of FAD-dependent glucose dehydrogenase using porous gold electrodes and enzymatically implanted platinum nanoclusters, Bioelectrochemistry 133 (2020), 107457, https://doi.org/10.1016/j.bioelechem.2020.107457.

[23] M. Kim, J. Kim, Effect of pH on anodic formation of nanoporous gold films in chloride solutions: optimization of anodization for ultrahigh porous structures, Langmuir 30 (2014) 4844–4851, https://doi.org/10.1021/la500732z.

[24] H. Jeong, J. Kim, Fabrication of nanoporous Au films with ultra-high surface area for sensitive electrochemical detection of glucose in the presence of Cl^-, Appl. Surf. Sci. 297 (2014) 84–88, https://doi.org/10.1016/j.apsusc.2014.01.082.

[25] K. Nishio, H. Masuda, Anodization of gold in oxalate solution to form a nanoporous black film, Angew. Chemie Int. Ed. 50 (2011) 1603–1607, https://doi.org/10.1002/anie.201005700.

[26] D. Ratautas, A. Laurynėnas, M. Dagys, L. Marcinkevičienė, R. Meškys, J. Kulys, High current, low redox potential mediatorless bioanode based on gold nanoparticles and glucose dehydrogenase from *Ewingella americana*, Electrochim. Acta 199 (2016) 254–260, https://doi.org/10.1016/j.electacta.2016.03.087.

[27] Y. Yi, G. Weinberg, M. Prenzel, M. Greiner, S. Heumann, S. Becker, R. Schlögl, Electrochemical corrosion of a glassy carbon electrode, Catal. Today 295 (2017) 32–40, https://doi.org/10.1016/j.cattod.2017.07.013.

[28] J.M. Levêque, L. Duclaux, J.N. Rouzaud, L. Reinert, N. Komatsu, A. Desforges, S. Afreen, M. Sivakumar, T. Kimura, Ultrasonic treatment of glassy carbon for nanoparticle preparation, Ultrason. Sonochem. 35 (2017) 615–622, https://doi.org/10.1016/j.ultsonch.2016.02.004.

[29] R. Žalnėravičius, V. Klimas, A. Naujokaitis, A. Jagminas, A. Ramanavičius, Development of biofuel cell based on anode modified by glucose oxidase, *Spirulina platensis*-based lysate and multi-walled carbon nanotubes, Electrochim. Acta 426 (2022), 140689, https://doi.org/10.1016/j.electacta.2022.140689.

[30] X. Xiao, P. Si, E. Magner, An overview of dealloyed nanoporous gold in bioelectrochemistry, Bioelectrochemistry 109 (2016) 117–126, https://doi.org/10.1016/j.bioelechem.2015.12.008.

[31] A. Othman, H.K. Bilan, E. Katz, O. Smutok, Highly porous gold electrodes - preparation and characterization, 9 (2022) e202200099. 10.1002/celc.202200099.

[32] C. Fisica, U. Milano, Real surface area measurements in electrochemistry, Pure & Appl. Chem. 63 (1991) 711–734, https://doi.org/10.1351/pac199163050711.

[33] M.D. Scanlon, U. Salaj-Kosla, S. Belochapkine, D. MacAodha, D. Leech, Y. Ding, E. Magner, Characterization of nanoporous gold electrodes for bioelectrochemical

applications, Langmuir 28 (2012) 2251–2261, https://doi.org/10.1021/la202945s.
[34] C.A. Martínez-Huitle, S. Ferro, A. De Battisti, Electrochemical incineration of oxalic acid: role of electrode material, Electrochim. Acta 49 (2004) 4027–4034, https://doi.org/10.1016/j.electacta.2004.01.083.
[35] Y. Deng, W. Huang, X. Chen, Z. Li, Facile fabrication of nanoporous gold film electrodes, Electrochem. Commun. 10 (2008) 810–813, https://doi.org/10.1016/j.elecom.2008.03.003.
[36] W.K. Paik, S. Han, W. Shin, Y. Kim, Adsorption of carboxylic acids on gold by anodic reaction, Langmuir 19 (2003) 4211–4216, https://doi.org/10.1021/la026836s.
[37] O.F. Odio, L. Lartundo-Rojas, P. Santiago-Jacinto, R. Martínez, E. Reguera, Sorption of gold by naked and thiol-capped magnetite nanoparticles: an XPS approach, J. Phys. Chem. C 118 (2014) 2776–2791, https://doi.org/10.1021/jp409653t.
[38] B.V. Crist, Handbook of monochromatic XPS spectra, John Wiley, Chichester, 2000.
[39] K. Juodkazis, J. Juodkazytė, V. Jasulaitienė, A. Lukinskas, B. Šebeka, XPS studies on the gold oxide surface layer formation, Electrochem. Commun. 2 (2000) 503–507, https://doi.org/10.1016/S1388-2481(00)00069-2.
[40] L. Lu, Y. Dong, J. Wang, Q. Li, X. Wu, Direct electrochemistry and bioelectrocatalysis of horseradish peroxidase entrapped in a self-supporting nanoporous gold electrode: a new strategy to improve the orientation of immobilized enzymes, Anal. Methods 7 (2015) 6686–6694, https://doi.org/10.1039/C5AY01333J.
[41] M. Hakamada, M. Takahashi, M. Mabuchi, Enzyme electrodes stabilized by monolayer-modified nanoporous Au for biofuel cells, Gold Bull. 45 (2012) 9–15, https://doi.org/10.1007/s13404-011-0038-1.
[42] J.A. Cracknell, K.A. Vincent, F.A. Armstrong, Enzymes as working or inspirational electrocatalysts for fuel cells and electrolysis, Chem. Rev. 108 (2008) 2439–2461, https://doi.org/10.1021/cr0680639.
[43] E. Ramonas, A. Shafaat, M. Dagys, T. Ruzgas, D. Ratautas, Revising catalytic 'acceleration' of enzymes on citrate-capped gold nanoparticles, J. Catal. 404 (2021) 570–578, https://doi.org/10.1016/j.jcat.2021.10.036.
[44] A. Baradoke, B. Jose, R. Pauliukaite, R.J. Forster, Properties of Anti-CA125 antibody layers on screen-printed carbon electrodes modified by gold and platinum nanostructures, Electrochim. Acta 306 (2019) 299–306, https://doi.org/10.1016/j.electacta.2019.03.081.